Skin Typing and High Resolution MRI of Human Skin: Multiple Contrast Approach for Image Characterization

Rakesh R.Sharma[1,@]

[1]*CIMAR, National High Magnetic Field Laboratory, Tallahassee, Florida and*
[1]*Departments of Chemical Engineering and Biomedical Engineering,*
FAMU-FSU College of Engineering, Tallahassee, Florida 32310;

Key word: Skin • Multiple contrast • Epidermis • Dermis • High Resolution • Microimaging
Running Title- High resolution MRI of Human Skin

[@]Correspondence to:

Rakesh Sharma, Ph.D
Departments of Chemical Engineering and Biomedical Engineering,
B222 F, FAMU-FSU College of Engineering,
2525 Pottsdamer Street,
Tallahassee, FL 32310
Email: rs05h@fsu.edu
Phone: (850) 590-1052

Abstract

***Background and objectives*:**

The *ex vivo* magnetic resonance microimaging (MRM) image characteristics are reported in human skin excised samples.

Design and methods:

Human excised skin samples were imaged using custom coil placed inside 500 MHz NMR imager for high resolution microimaging. Skin *in vivo*- and *ex vivo* MRI images were processed for characterization of different skin structures. Contiguous cross-sectional T1-weighted 3D spin echo MRI, T2-weighted 3D spin echo MRI and proton density images were compared with skin histopathology and NMR peaks. In all skin specimens, epidermis and dermis thickening and hair follicle size was measured using MRM.

Results:

Optimized TE and TR parameters and multicontrast enhancement generated better MRI visibility of different skin components. Within high MR signal regions near to custom coil, MRI images at short echo time were comparable with digitized histological sections for skin structures of

epidermis, dermis, hair follicles in 6 (67%) of the 9 specimens from different age groups. Skin % tissue composition, measurement of epidermis, dermis, sebaceous gland and hair follicle size, skin NMR peaks were signatures of skin type. The image processing determined the dimensionality of skin tissue components and skin typing in different age groups.

Conclusion: The ex vivo MRI images and histopathology of skin may measure the skin structures and skin NMR peaks with image processing may be tool for determining skin age typing and skin composition.

Introduction

Human skin tissue microimaging evaluation was reported first time by Bittoun et al. 1990 using one-axis planar gradient insert to achieve high resolution in perpendicular direction to skin surface with voxel size 18x312x1000 micrometers for the identification of sebaceous glands, smooth epidermis and continuous dermis with distinct hair follicles wrapped up with epidermis layers [1]. However, the large pixel size in second and third dimensions and low spatial resolution always

remained a challenge to visualize collagen rich dermis [2]. Partly, the problem was solved by axial resolution enhancement 11 micrometers by using high bandwidth setting and lateral resolution enhancement 30 micrometers at center frequency and transducer aperture [2]. However, enhanced detection and sensitivity to offset signal-to-noise ratio (SNR) loss, short T2 relaxation constants, and low proton density due to bound water, low resolution and contrast are still major problems to visualize skin components by MRI. The sebaceous glands and subcutaneous fats are understood to generate sufficient phase contrast as identifiable by T2 weighted images [2, 3]. The outermost layer epidermis (100 micrometers thick) covers dermis (3 millimeters thick) in the skin. Dermis is composed of 65% water bound with 25% collagen and other 10% ground extracellular matrix [4]. The lipids in skin are visible and distinct by MRI. The visualization by in vivo/ex vivo MR microimaging (MRM) at higher magnetic field is emerging as a noninvasive modality of pixel by pixel contrast enhancement in skin evaluation for typing, characterization of skin lesions [5]. The purpose of this paper was: 1. to evaluate human skin samples by 500 MHz MRI visible skin features of epidermis-dermis and hair follicle features at optimized MRI scan parameters with enhanced multi-contrast using fast 3D variable flip angle gradient and multislice multiecho pulse sequences in less time; 2. to enhance contrast using external coil; 3. to compare the MRI visible skin features in different skin age groups with morphometric histology features; and NMR peaks; and 4. skin typing by postprocessing the topology of skin surfaces in different skin age groups.

Materials and Methods

Skin samples: The human normal skin MRI images[1] were analyzed from different age groups. Excised skins of dorsal calf tissue was received from the human abdomen either lateral sides of fresh male cadaver (35 years) at Southeast tissue alliance, Tallahassee.

3D FLASH and 3D MSME imaging pulse sequences

The low resolution 3D FLASH (fast large-angle spin echo) localizer with 60 degree partial flip angle and 3D MSME_Bio (PARAVISION 3.2) have distinct two pulse sequence sections i.e. slice selection and imaging encoding as described in PRAVISION 3.2 Bruker-Biospin, Bellerica, MA. 3D FLASH sequence has features of split slice and pulse encoding gradients, asymmetric echo and a slab-selective minimum-phase Shinner-Le Roux pulse. It served as localizer [6].

3D MSME has features to acquire the 3D proton density images. The sequence used the radiofrequency (Rf) pulse that generated resonance spread over a wider slab of skin tissue of 2.6 mm^3 to generate images in three planes of axial, coronal and sagittal planes [5].

[1] The author got TCC imaging internship training at Tallahassee Memorial Hospital under supervision of Dean CJ Chen.

High Resolution Multislice Multi Echo (MSME_Bio) sequence

The high-resolution multislice-multiecho-Bio sequence (PARAVISION 3.2) has two distinct sections: slice selection and image encoding. The MSME-Bio sequence had features of 2D imaging in single plane. This sequence used a radiofrequency (RF) pulse, which generated resonance spread over a thin band of tissue to give off a magnetic resonance detectible signal. Images were acquired as 2D slices. For skin imaging, the MSME-Bio PARAVISION 3.2 sequence was applied many times in rapid succession so that spin-echo lasts for 8 msec at slew rate 15 mTesla/meter in volume of interest (VOI) = 0.002 mm^3. During each echo application the amplitude of the phase encoding gradient was stepped up to a new phase encoding value. Slices were acquired in contiguous manner while the slices were selected in rapid succession. There was no motion between adjacent slices that provided reasonable continuity of skin images between slices.

Multiple contrast protocol

With a multiple contrast protocol using T1-weighted, proton density-weighted and T2-weighted images, area of skin epidermis and dermis features were distinguished and measured [5].

Contrast enhancement and 3D graphic curves for MR microimaging at 11.7 T

To generate contrast enhancement plots of different skin structures, the human skin samples > 2 mm^3 volume were obtained fresh in saline and later cold packed for immediate MR imaging (n = 8). For scan parameters optimization, 11.7 T multi-slice multi-echo (MSME) images were obtained on

'Bruker Bio-spin 500 Utility' at 7 discrete echo times (TE = 10 - 80 ms) with repetition time (TR = 4 sec) and 8 transients per acquisition. The TE and TR values were plotted in 3D to get 3D graphic curves.

With skin sample position maintained in local RX custom coil, an additional image data set was collected at TE = 20 ms and TR arrayed at 8 discrete delays (300 - 8000 ms) for achieving saturation recovery. This optimized image set was also analyzed to yield a parametric T1 signal intensity distribution image for selected skin slices.

A 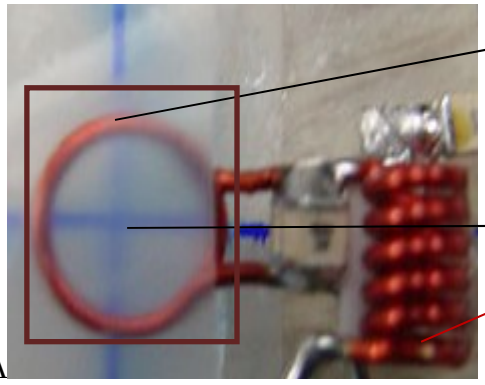

A customized local surface RX coil made of 2 mm thick copper for generating high SNR in the regions close with coil. It acts as high temperature sensitive Rf coil with high Q and high SNR for the skin MRI microimaging[1].

Region of homogeneous high point-spread-function As shown in panels B.

Connection of Rf coil with capacitor connected with

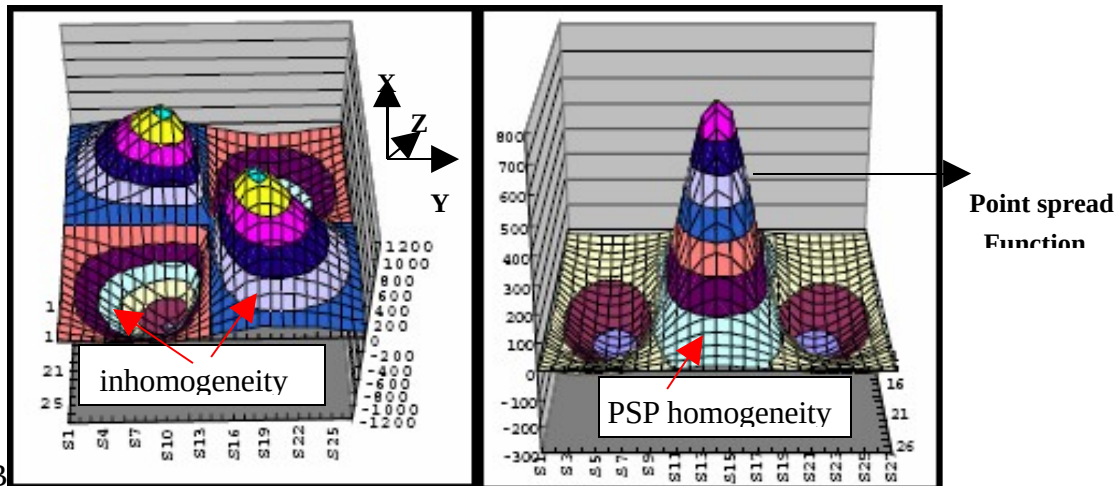

Figure 1: (on top panel A). local RX coil to enhance the SNR signal; and (at bottom panel B): Homogeneity peak characteristics with a constraint of target field, a current pattern shows x, y and z gradients of RX coil to achieve 10 gauss/cm gradient strength using matrix equation for 5 mm region of interest[2].

Coil for signal enhancement

For high resolution and SNR in skin microscopic MR imaging, an integrated planar-type gradient coil integrated with RX coil was used in determining spatial signal characterization and preoperative typing of skin [7]. The distribution of discrete current elements in mesh shown in equation 4 were optimized to provide spatial information of MR images keeping Gx, Gy and Gz constant within volume of interest as shown in equations (1), (2) and (3).

$$Gx = \partial Bz/\partial x \qquad (1)$$

$$Gy=\partial Bz/\partial y \qquad (2)$$

$$Gz=\partial Bz/\partial z \qquad (3)$$

[2] Point spread function is the characteristic of RX coil performance as principles defined in ISMRM '04 [7].

The current 'c' distribution in the gradient coil for minimum power use can be calculated as

$$c = W^{-1}G^{T}\, k[GW^{-1}GT]^{-It} \qquad (4)$$

where 'c' is loop current, I is line current, G is field at target position, W is energy dissipated in time 't', T is temperature, I is target field of target position and k is conversion matrix. It gives the matrix of desired current as shown in Figure 3 B for minimum power usage and output of high MR signal intensity.

These images sets were analyzed by NIH Image J 1.63 and Optimas 6.5 software to produce a parametric T2 image for selected slices. T2 calculations were performed on a voxel by voxel basis by applying weighted linear regression analysis on the voxel signal intensities.

Tissue preparation for human skin histopathology and skin NMR spectroscopy:

The skin samples were immediately processed for histology and NMR spectroscopy soon after MR imaging was completed. The skin samples were cut into 8 serial 2.5-mm segments matching with corresponding MR images. Using landmark hair follicle as feucidial marker, other skin

structures were coregistered. For histological examination, skin samples were made free from fibers and decalcified in 1% formalin, 4-micron sections were cut, mounted and processed for staining with hematoxylin-eosin staining of neutral lipids, fibrous and cellular skin components. The morphology of human skin pathological changes was assessed using by ImagePro® attached photo scanner at 350 dpi. Each single skin image was scanned for the different skin MRI features (n = 8). Exact diameter of hair follicle and hair stalk on histopathology slide was measured by view-scale to create absolute scale. Outer radius and follicle thickness ratio were measured from hair radius and area on MR images and matched with histopathology features on skin sections [8].

The height of the hair follicle of each skin was measured. The total extent of dermis and epidermis was assessed by the skin viability index [8]. The visible oil glands, hair follicle area, fibers and keratin-glycolipid rich areas in skin were identified to obtain skin viability score. Skin viability score for each skin sample divided by dry skin thickness was measured for the skin grading [8]. Skin sections were stained with Hematoxylin & Eosin for skin morphology and its structures. Skins had overlying swollen epidermis. Young and healthy skin samples in skin type I or grade 1 skin had intact epidermis and dermis structures [5].

"Skin epidermal thickness" burden (SET) and skin viability:

MRM images were manually traced for outer and inner epidermis surfaces for its area measurement. The area measurements of epidermis determined the skin 'SET' burden = (Outer surface size – inner surface size) x 100%. The hair follicle determined the percent skin viability

[hair follicle radius / hair follicle area x 100%]. These calculations were performed on the human skin MR images showing distinct skin structures. The corresponding histological sections of the skin stained with trichrome-mason were put on a projecting microscope (Microprojector model KZ-5, Carl Zeiss, Inc) and were projected onto a digitizing table. The size of skin appendages viz. hair follicle, sebaceous gland, sweat gland, epidermis and dermis fibrous features were manually traced and quantified by using NIH Image J1.63 Analysis Software program. The 'SET' and percent skin viability were determined by histopathology in the same manner as described above for MRI. By using the hair follicle and inner epidermis surface as the points of reference, comparative analyses were performed with the MRI scans at the same level [5, 7, 8].

Skin NMR spectroscopy:

After MR microimaging, some skin samples corresponding with histology were used for perchloric acid extraction to visualized amino acid peaks by proton NMR spectra as previously described [9]. Briefly, Six skin 2 mm pieces (0.1 to 0.15 grams wet weight) were frozen in liquid nitrogen and stored at -70°C. The finely ground powder was extracted by addition of 2 volumes of

ice-cold 5% PCA per gram wet weight (w/v) of tissue, followed by agitated on a vertex for 1 min and centrifuged (14,500 gram, 4°C, 20 min) to get pellet and supernatant. The supernatants were neutralized with potassium bicarbonate, centrifuged (14,500 g, 4°C, 30 min), and lypholized. The lypholized extracts were dissolved in 0.5 ml D_2O (99.8% D) and the pH adjusted to 0.2% DCl(99.5% D) and 0.2% NaOD (99.5% D). Spectra were obtained using 5 mm tubes by Fourier Transform NMR on Bruker AM-500 spectrometers operating at frequency of 500 MHz and temperature 20-22°C. The residual HDO (solvent peak) was suppressed by a weak saturating pulse irradiating for 1 sec during pulse delays. One dimensional spectral conditions operating at 500 MHz were 45 flip angle, 4000 Hz spectral width, 16 K data points, 500 microsec pulse delay time and 2 sec recycle time. Chemical shifts were measured for different amino acid ratios of glutamate:serine, creatine:glycine, taurine/alanine, valine:leucine/isoleucine, phosphorylcholine/glycerophosphorylcholine:alanine, and lactate:alanine ratio in reference to the methyl hydrogen resonance of 3-(trimethyl silyl)-tetradeutero sodium propionate (TSP).

MR microimaging and histology correlation and image post-processing:

MR images were processed for high contrast using 'Sun VNMR' software. These images were displayed on a Silicon Graphics SGI Octane 2 workstation. Similarly, histology slides were photographed with Olympus D-320 L Digital Vision camera attached high field microscope and the colored digital images were projected with a microimage Video system and Ikegami 370 M

control unit onto a SONY Trinitron super fine pitch screen for area computation using Optimas 6.5 software. Data for histology and MR images were compared and statistically analyzed using PRISM 3 software [5, 10]. The active contour method was used to visualize skin surface topography as reported elsewhere [26]. The skin surface texturization and contour analysis was done as described elsewhere [27].

Sensitivity and Specificity:

The sensitivity and specificity testing was done as final MRI criteria for evaluation of T2-weighted parametric images. Different MRI signal intensities of different skin appendages on gray scale represented the sensitivity. The specific skin structures displayed the distinct and different T1 weighted MRI signal intensities on MSME-Bio spin echo method (TE = 15 ms) and T2 weighted (TE = 50 ms).

Statistical Analysis

For optimization, MRI data were reported as % signal intensities. MRI and histology data were

reported as mean ± 1 sd. Comparison was done by percent difference and correlations were made by paired t test, least-squares linear regression. Differences were significant if the two-foiled value was < 0.05 [5].

Results

MR imaging and human skin specimens:

In vivo FLASH MR images obtained with 2.5 cm surface coil placed over skin surface to acquire images in voxel size = 15 x 65 x 500 micrometers, displayed hyperintense epidermis, hypointense papillary dermis and remnants of fatty hypodermis shown in Figure 2 in panel 1. 3D FLASH spin echo image enlarged view showed main three skin features as shown with arrows in panel 1. For clear visibility, panel 1 highlights the epidermis and hair follicle features (shown with arrows in Figure 2). Each skin structure showed specific signal intensity (T1 = 1000 ms; T2 = 30 ms for epidermis) at different T1/T2 and proton density weighting. MSME_Bio images showed epidermis as bright (panels 2 and 3). Proton density weighted image in same imaging session showed distinct skin structures (see Figure 2 in panel 2). T2 weighted image showed better contrast between skin structures (see Figure 2 in panel 3). T1 weighted image showed better darker structures (see Figure 2 in panel 4).

Ex vivo multicontrast MRI images of excised skin specimens were obtained from intact skin tissue removed from hypodermis in different skin age subjects as shown in Figure 3.

Multicontrast MRI imaging of skin:

Selection of MRI image scan parameters generated three T1-weighted, T2-weighted and proton density-weighted images that further enhanced the contrast. Proton density images are shown in Figure 3 with skin structures (arrows on panels in rows). In Figure 3, proton density-weighted image of normal skin (panel A); skin grade 1 (panel B), grade 2 (panel C), grade 3 (panel D) and grade 4 (panel E) is shown. These skin structures offered a possibility of measure swollen epidermis burden and skin viability. The epidermis and hair follicle thickness measurement in a normal skin sample distinguished the different skin types or 'skin grades'. Skin grade empirically reflects the skin viability and age. The distinct thin epidermis and complete hair follicle area were seen (panels A-C) in high-grade skin in young age (20-35 years) while broken or missing or swollen epidermis and incomplete hair follicle area were seen (panels D-E) in low grade skin in

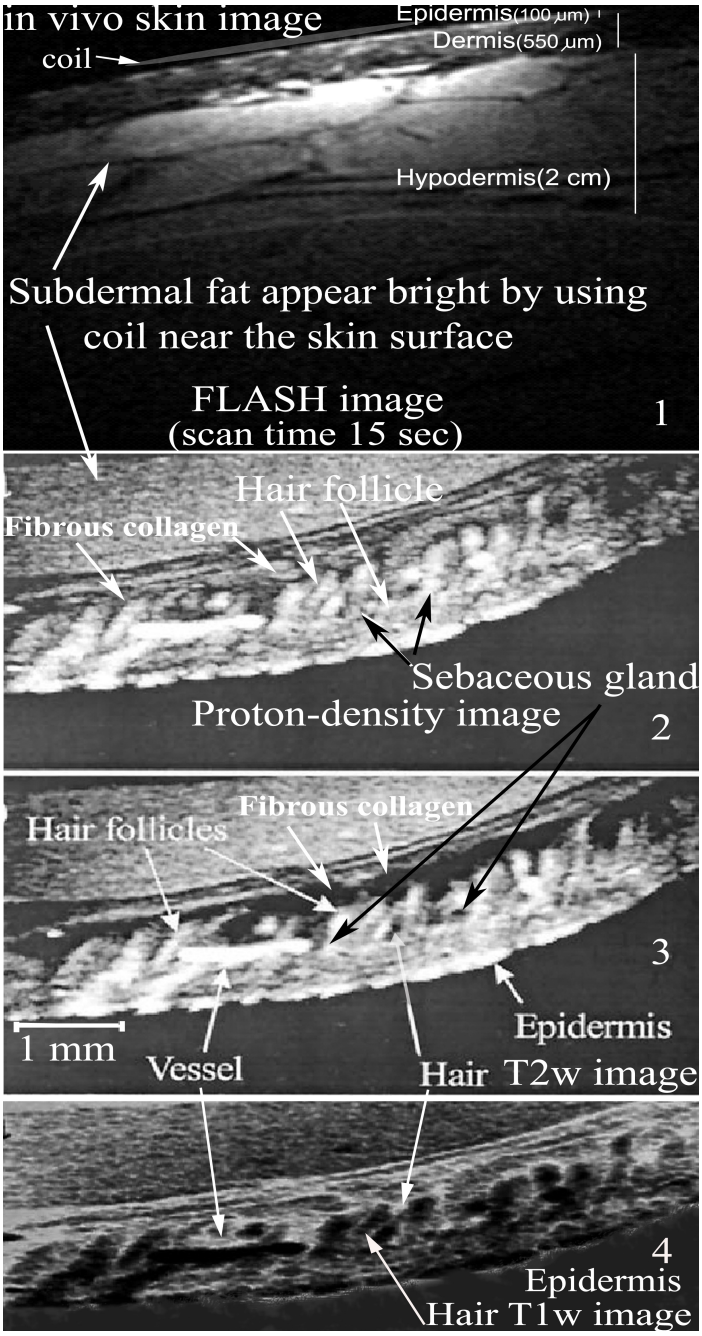

Figure 2: An in vivo skin image is shown. A surface coil was used near the skin surface to enhance the MR signal intensity at low TE/TR (T1-w) with high signal-to-noise ratio of subdermal lipids (shown in top panel 1). Scan parameters were: TE=5 ms, TR=100 ms, matrix = 125 x 256, NEX = 2, FOV = 15 x 65 x 500 for FLASH image. Image shows distinct fat with epidermis, dermis and hair follicles as shown by arrows (see panel 1). Proton density image at short TE shows distinct vascular structures of vessels, deep seated hair follicles, distinct and isointense fibrous tissue (see panel 2) different from T2-weighted image showing better contrast of darker fibrous tissue and brighter sebaceous glands, hair follicle isointense and brighter vasculature (see panel 3); and T1-weighted image showing darker hair follicle and vasculature(see panel 4).

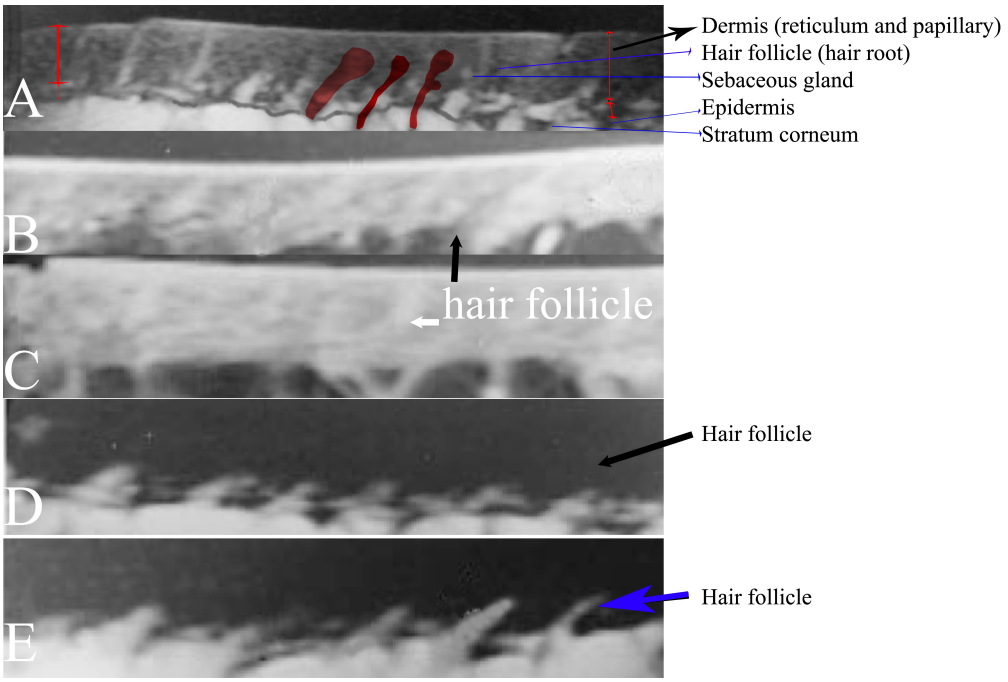

Figure 3: ex vivo skin proton density image is shown of normal skin (panel A); skin grade 1 (panel B), grade 2 (panel C), grade 3 (panel D) and grade 4 (panel E). Notice the difference in appearance of hair and dermis structures embedding collagen fibers and dermis dtructures. Hair follicles degenerate with skin age with hardening of follicles.

its cross-sectional magnetic resonance images (36-60 years or beyond). Interesting observation was darkened areas of fat rich regions and missed hair follicles. Deep skin cracks were distinct (see panel E). The dermis showed hypointensity on MRI and low cell density, high vascular dermis and oil rich hair follicle on histology were also sign of high skin grade as shown in Figure 3 (panel A).

Quantitation of skin structures:

The mean score of SET was greater in human skin specimens. The measurements of skin structures, as revealed by micrometer, were distinct in the normal fresh skin (see Table 1). A variable degree of dermis thickening was observed in skin, as revealed by paraffin sections of skin. Hair follicle, hair stalk, sebaceous gland, stratum corneum, epidermis layer were observed in skin tissue. However, skin showed epidermis thickness and its degeneration with age as loss of skin grade. On histology, skin sample showed evidence of epidermis and hair follicle size, as indicated by thickening characteristics.

The skin grade 0 revealed that normal human skin showed significantly intact epidermis, quite distinct prominent hair follicle, indicating intact viable characteristic of skin. Assessment in general was based on the skin appearance. It revealed the thickness of epidermis and hair follicle shape as fragile or incomplete as main identification marker of poor skin viability and low grade.

Comparison and analysis of the histologic and ex-vivo MRI features of human skin Images:

A contiguous series of representative ex vivo MR microimaging (MRM) slices 0.5 mm thick with in-plane resolution of 0.5 mm is shown (Figure 4). These skin image slices enabled the identification of heterogeneous skin structures appearing as dark, gray and bright areas. In these skin images, extensive viable epidermis showed as darker and stratum corneum showed brighter (Figure 3). Prominent hair follicle (~0.25 mm diameter) was surrounded by outer sheath made of epidermal cells, hair sebaceous gland diameter (0.05 - 0.15 mm), circular hair root diameter (1.0

-1.5 mm) surrounded with massive dermis reticular accumulations (100 – 150 micrometers) and high density cutaneous vasculature structures in dermis with SNR = 7. MRM visualized (Figure 4, panel on top) specific features of lipid rich stratum corneum and dermis regions, with specific shapes of sweat glands in vascular rich dermis layer at SNR = 13. Down the dermis, fat rich adipose tissue was distinct due to its fat-water phase difference. Figure 4 shows skin magnetic resonance images across the coronal plane and transaxial plane at different levels of slice sections, with each showing a straight-curved pine shaped hair. The corresponding histological sections confirmed the features such as hair body with follicle, root, sebaceous gland, sweat gland, covered by viable epidermis within the dermis, epidermis and coming out the stratum corneum (Figure 4, panel on bottom). The SET and hair characteristics were also seen in MRI image and confirmed by histological analyses of the corresponding sections. Water-fat interface was distinguished as black or no signal (see Figure 2) that showed lipid rich regions in histology sections.

Table 1: Comparison of histomorphometric measurements and ex vivo MRI visible skin structures of different skin types. Skin type I (age <20 years) shown by (A); skin type II(age 20-35 years shown by (B); skin type III (age 36-60 years) shown by (C); and skin type IV(age 60 and above) shown by (D) for different skin structures of stratum corneum (mm), epidermis (mm x 10), dermis (mm), hair size(mm) and hair follicle thickness (mm) shown in Figure 4. Different skin structures showed comparable size by both MRI and histology.

Skin MRI[a] / Skin histology[b]	Total skin size and area					% viability	Hair follicle size	
	Epidermis		Dermis		Stratum Corneum	Hair size		
	Thickness	Area	Thickness	Area		Thickness	Area	
% difference	(mm)x 10	(mm²)	(mm)	(mm²)	(mm)	(mm)	(mm)	(mm)
Type I(A)	1.70	9.08	1.47	6.79	25.22	0.72	12.4	1.95
115_seg0.5	1.69	8.97	1.46	6.69	25.93	0.68	10.0	1.92
% difference	**1.00**	**1.20**	**0.68**	**10.0**	**2.73**			**1.53**
Type II(B)	1.69	8.97	1.42	6.33	29.43	0.82	12.9	2.10
120_seg1.5	1.68	8.87	1.41	6.24	29.65	0.78	12.5	1.99
% difference	**1.00**	**1.11**	**0.70**	**1.42**	**0.74**	**4.87**	**3.10**	**5.24**
Type III(C)	1.68	8.87	1.42	6.33	28.63	0.92	14.50	2.50
123_seg1.5	1.67	8.76	1.39	6.07	30.70	0.86	14.16	2.60
% difference	**1.00**	**1.24**	**2.11**	**4.10**	**7.23**	**6.52**	**2.34**	**3.84**
Type IV(D)	0.35	8.76	1.20	6.10	23.50	0.75	14.50	2.50
130_seg1.5	0.32	8.74	1.20	6.05	23.44	0.74	14.20	2.45
%difference	**3.0**	**2.00**	**0.0**	**5.00**	**6.00**	**1.00**	**30.0**	**5.0**

[a]Skin structures measured by magnetic resonance microimage (1 mm thick).

[b]Skin structures measured by histology corresponding MRM slice(1 mm thick).

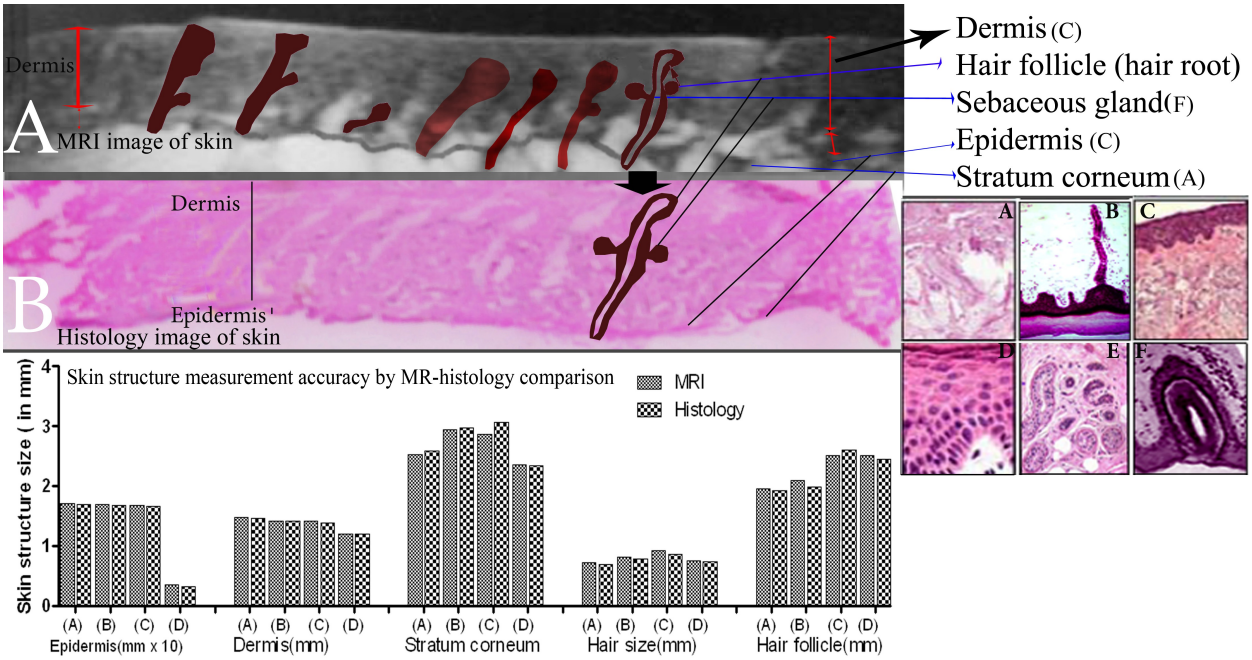

Figure 4: Comparison of skin MR image and histology digital image for measurement of area of epidermis, hair follicle, sebaceous gland. Different skin structures are shown in MRI proton density weighted images (panel A); in histology images (panel B) with different skin structures in inserts(A-F). The measurement of different skin structures showed comparable skin structure areas but histology measured less due to shrinkage of tissue in pathological processing as shown at the bottom on left.

Quantitative comparison of total hair area, thickness of the hair root, epidermis area from MRM and histological samples was made as shown in Table 1 and histogram bars (at bottom) and corresponding correlation (Figure 4). The MRM values and the histological values showed correlation shown in Figure 4. The linear regression was calculated for epidermis areas ($r^2 = 0.498$; p value 0.0048); and hair follicle areas ($r^2 = 0.881$; $p < 0.0001$) to calculate % SET ($r^2 = 0.831$; $p < 0.0001$). The percent "epidermis thickness" or % SET was (mean $\pm$ sd) determined by comparing skin epidermis MRM with their respective histology digital images. The location of stratum corneum was defined as the most outer layer and adipose tissue as innermost layer of the skin. Hair area showed significant correlation ($r^2 = 0.137$; $p < 0.193$) between histology and MRI. Similarly, there was a correlation ($r^2 = 0.771$; $p < 0.0001$) between epidermis area by MRM and histology. The total epidermis and dermis area measurement showed correlation by T2-w MRM ($r^2 = 0.646$; p 0.008) with histology.

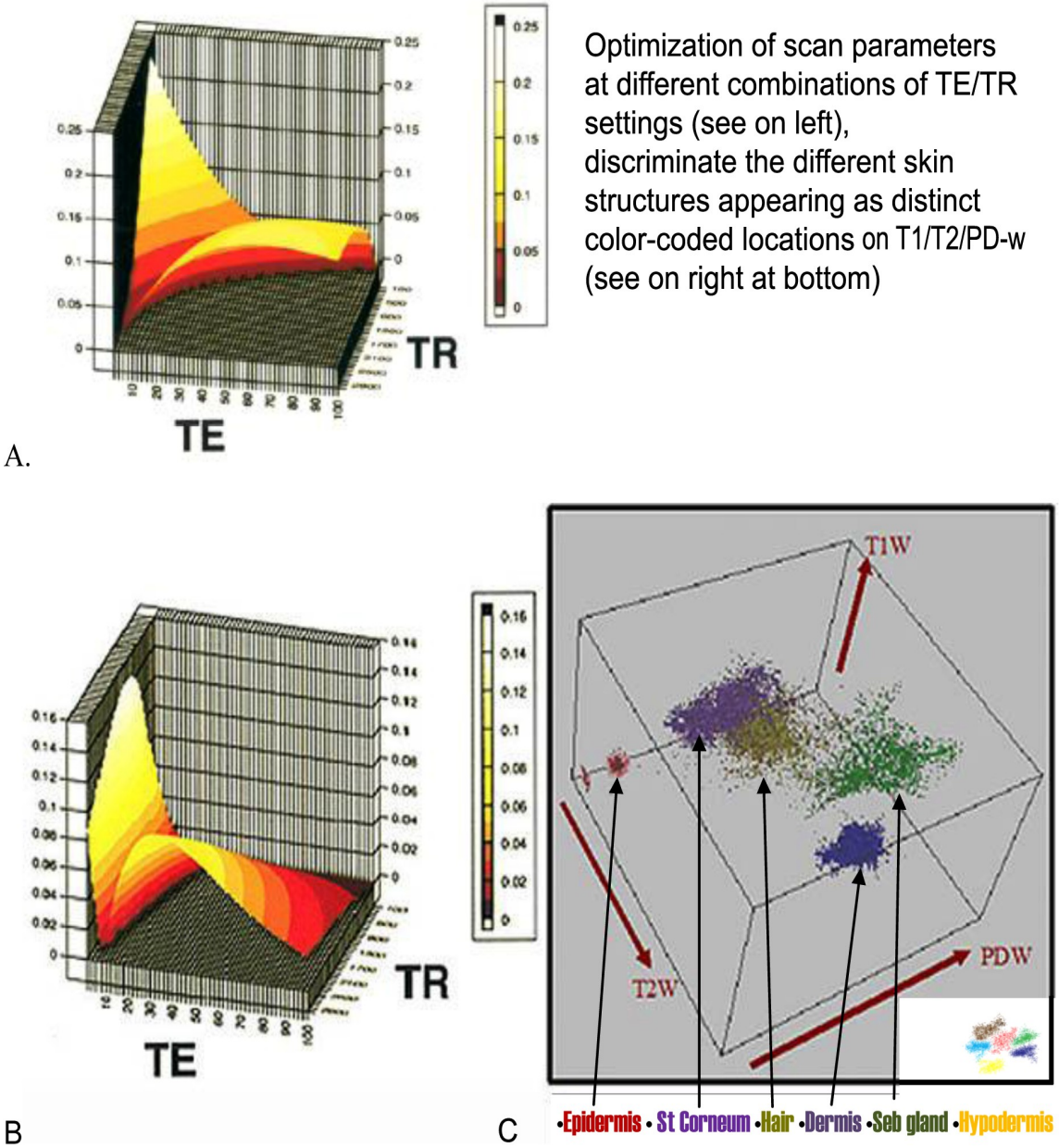

Figure 5: A physical relationship between echo time (TE) and repetition time (TR), is shown on 3D graphs to construct parametric T1 image. (On top left side) Optimization of scan parameters TE and TR is shown at different time points to achieve a set of selective MRI signal intensity M_{xy} showing longitudinal relaxation weighting (T1-w) at low TE/TR or transverse relaxation weighting (T2-w) at higher TE/TR or proton density weighting (PD-w) at low TE and higher TR (see panel A). At very low TE, MRI signal intensity varies showing heavy T1-w images (see panel B). Different skin structures show discrimination due to their distinct behavior at different T1-w/T2-w/PD-w sensitivity. Epidermis shows low signal on all T1-w/T2-w/PD-w combinations while lipid rich sebaceous gland shows high signal on T1-w images (see panel C). The 3D discrimination of color-coded skin structures views a quick guide of skin structure identification and preference of T1/T2/PD-w in x,y, and z directions on images.

Table 2: Optimization of MRI spin echo parameters TE and TR for T2 parametric contrast enhancement between glycoloipid and viable epidermis skin tissue at 11.7 T (see Figure 5). Different combinations of TE and TR generate T1-, proton density- and T2- weighting and their relative appearance on gray scale.

TR (ms)	TE (ms)	MRI Signal Intensity on gray scale
2000	10-30	dark; heavy T1 wt
2000	20-40, 50- 80	gray; medium T1 wt
1000	2-10	bright; T2 wt
1000	30-70	dark; heavy T1 wt
800	10-20	gray; medium T1 wt
200	20-70	dark; heavy T1 wt

Contrast enhancement and resolution:

Two approaches were used to improve resolution viz. 3D plots for hair rich skin tissue at 11.7 T and parametric imaging. Figure 5 and Table 2 show 3D plots revealing that a high contrast of 0.25 can be achieved using a T1-weighted imaging at very short TE (~4 ms) and short TR (~ 500 ms) and lower contrast of ~0.12 may be obtained by T2- weighted imaging at more accessible parameters TR = 2-3 sec; TE = 50-100 ms.

In second ‘discriminate analysis’ multicontrast approach, T1-weighted, T2-weighted and proton density-weighted image intensities categorized skin tissue structures with color display (right panel of Figure 5). With a multicontrast protocol using T1-weighted, T2-weighted images and proton density-weighted images showed skin structures as shown in Figure 5. Image intensities of different locations on these skin images indicated that some areas were MRI-visible on T1-weighted, T2-weighted or proton density weighted images. So, gray levels at any location on these images may characterize skin vascularity and fibrous rich regions by combining the contrast information of that location on these three images.

Rakesh Sharma

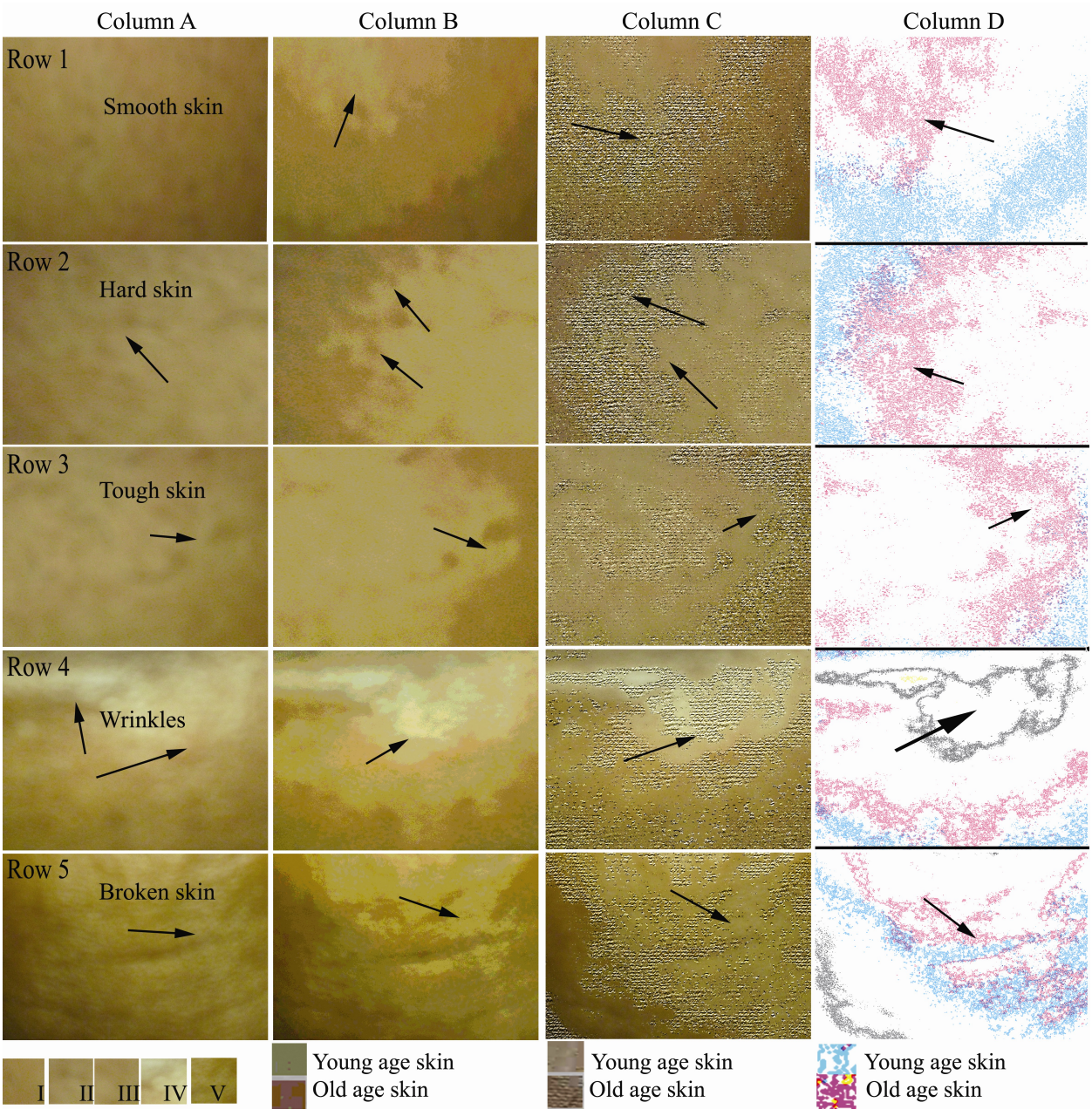

Figure 6: Different skin type I-IV skin surface optical camera ready images are shown from abdomen. Notice the difference in their appearance by skin surface of a healthy volunteer age 16 years (row 1); age 26 years (row 2); age 35 years (row 3); age 55 years (row 4); and age 65 years (row 5) in column A. Skin surface topography by posterization on column B shows gradation of smoothness or tone in different ages (see rows 1-5 for changes in color in some areas) . Skin surface texturization by texture analysis in column C shows the lifted skin surfaces increasing with age seen as distinct areas (see rows 1-5 for changes in color in some areas). Skin surface contours by contour analysis in column D shows the skin roughness or wrinckle as color-coded regions increasing with age (see rows 1-5 for changes in color in some areas). Skin surface characteristics in different age groups also defined skin grades. Grade 0(<20 years); Grade 1(20-30 years); Grade 2(31-45 years); Grade 3(46-60 years); Grade 4(61 years and above).

Image processing and skin typing

The skin typing criteria including skin texture, skin contour and skin typography showed the distinct visual appearance of skin surface as shown in Figure 6. The skin typing was based on two factors: skin smooth surface and number of skin hairs in unit surface area. The skin type 0(excellent in <20 years); skin type I(superior in age 20-30 years), if variation of skin surface is minimum with minimum hair in unit skin surface area; skin type II(good in age 31-45 years), if skin surface variation is less than 50% with 4-5 hairs in skin surface of 1 cm^2; and skin type III(fair in 46-60 years) and skin type IV(poor in 61 years and above), if skin surface variation is more than 50% with 10 or more hairs in skin surface of 1 cm^2. The appearance of stratum corneum surface and hair origin on surface indicated the utility of skin typing as quick skin evaluation useful in cosmetics and dermatology.

Skin measurements on images showed different structures contributed in each structure area to calculate total area. MRI signal intensities of each skin structures contributed to measure skin

structures. Some skin structures were not very clear and measurable to use them as morphometric parameters. Skin in old age showed less distinct hair follicle.

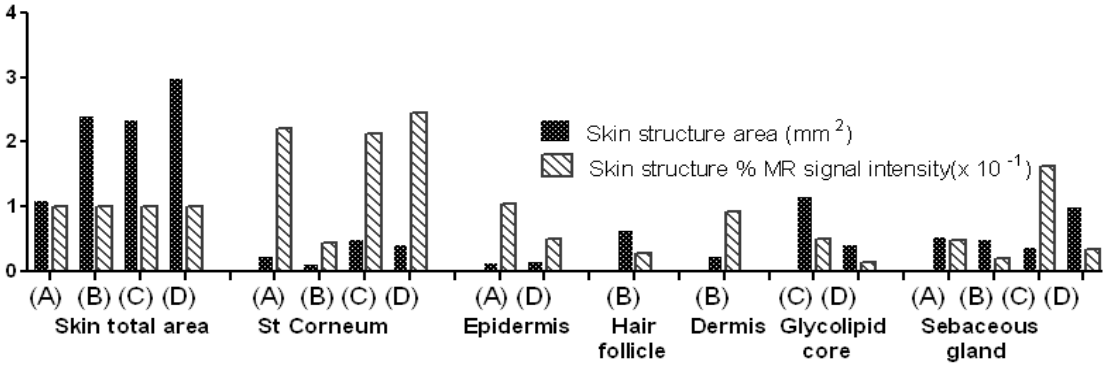

Figure 7: The figure represents the contribution of different skin structures in area measurement on proton density image and % MRI proton density weighted signal intensity in different skin age types (A), (B), (C), (D) in different age groups. The data shows a quick view to evaluate the visible MRI signal intensity of each skin structure as true representative of skin structure morphometry.

Table 3: The Table represents the contribution of each skin structure in skin measured area (in mm^2) of each skin structure and % MR signal intensity (in I.U.) of different skin structures i.e. epidermis, dermis, hair follicle, glycolipid core and sebaceous gland in four different skin samples of skin grades 1-4 (A,B,C and D) shown in Figure 3. Combined multi-contrast ex vivo PD weighted, T1 weighted and T2 weighted MR images were used for contrast and PD weighted images for area measurement of each skin structure and its % MR signal intensity (in arbitrary units) showing it highest MRI visible structures.

Structure	Area of constituents(mm^2)	% MR Signal Intensity(I.U.)

	A	B	C	D	A	B	C	D
Total skin area	1.1	2.41	2.34	2.98	100	100	100	100
St Corneum	0.24	1.09	0.49	0.42	21.8	4.5	21.3	24.5
Epidermis	0.14	--	--	0.16	10.4	--	--	5.1
Hair follicle	--	0.65	--	--	--	2.7	--	--
Dermis	--	0.24	--	--	--	9.3	--	--
Glycolipid Core	--	--	1.17	0.42	--	--	5.0	1.4
Sebaceous gland	0.54	0.50	0.38	1.00	4.9	2.1	16.2	3.3
Unclassified Core	0.23	0.55	0.27	0.19	--	--	--	--

Sensitivity and specificity: Table 4 shows the results of the relative signal intensity (CV %), sensitivity and specificity of the MRI criteria for evaluation of T2 weighted parametric images of skin (panels at bottom of Figure 5). Dermal vascular structures showed lowest sensitivity. However, fibrous regions next to hair and sebaceous gland were poorly visible on MRI because of dark areas of hair follicle. Other regions of collagen, lipid, and fibrous features were MRI visible and distinct by histology examination.

Table 4: Sensitivity and specificity of ex vivo skin MRI at spin echo (TE = 15 ms, TR = 1500 ms) and proton density image (panel on right). Different skin features are represented with reference to skin image for distinct skin components and corresponding T2 parametric image (A) of skin specimen and right postsegmented image (B) showing different signal intensities (CV %) and their relative appearance on gray scale with varying T2 ranges for different atheroma components.

Skin features	Signal intensity (CV %)	Sensitivity (%)	Specificity (%)	T2-wt (TE=15 ms)
S.Corneum	Dark	100	100	Dark
Epidermis	14.5(18 %)	95	85	Bright
Hair Follicle				
Dermis	23.0(7.5 %)	90	75	Dark
Glycolipid core	27.5(7.5%)	100	100	Gray
Sebaceous gland	35.5 (7 %)	85	90	Bright
Elastin	40.7 (13.5 %)	70	80	Gray

Table 5 summarizes the relative ex vivo MRI visibility of different excised tissue components using T1-, T2-weighted and proton density weighted (multicontrast) approach.

Table 5: The table represents different skin structures and their MRI visible protons in active chemical groups. These different constituents exhibit specific MRI signal intensity determined by their specific relaxation times T1 and T2 at specific 11.7 T magnetic field.

Skin components	Chemical structure	T1(ms) $S=N(1-e^{-T1/TR})$	T2(ms) $S=N(1-e^{-TE/TR})$	MRI Visibility* T1-w	T2-w	PD-w
Glycolipid	$-CH_2-CH_2-$	1643.3±25.6	52.9±2.5	+	-	+/-
Cholesterol	$-CH_3$	643.5±34.5	14.3±0.9	+	+/-	+/-
Keratin	Bound form	56.5±10	2.2±0.4	--	--	--
Collagen	$-CH_2$(-Gly-Hyp-Pro-)	1750.4±25.4	54.1±0.8	+	+/-	+
Elastin	$-CH_2-NH_2$	1640.6±16.2	62.2±1.1	+/-	+/-	+
Melanin	Paramagnetic	1204.2±14.4	16.0±1.2	+	-	-

* The relative gray scale MR signal intensity is shown as +(bright hyperintense), +/-(gray isointense), -(dark hypointense) on T1-weighted, T2-weighted and proton density(PD) weighted images.

Skin NMR spectroscopy:

At pH 4.0, expanded spectra of 0.8 to 4.5 ppm showed different metabolites. The vertical scale was standardized to tissue wet weight for proper comparison. At 500 MHz, the resonances of many small molecular weight compounds in all PCA extracts were resolved to reveal signals for various

amino acids and other metabolites including lactate, creatine, fatty acids (phosphorylcholine, glycerophosphorylcholine), and nucleotides. Using reference NMR assignment peak positions, peaks were identified and peak ratios showed following differences: (- CH_3) Ala peak intensity occurring at 1.46 ppm. In the 1 ppm region, (- , ' - CH_3)Val: (- , ' - CH_3)Leu/Ile peak intensity ratio; (N-CH_3)PC/(N-CH_3)GPC:(- CH_3) Ala; (- CH) Glu: (- , - CH) Ser peak ratio; (- CH_3) lactate: (- CH_3) Ala ratio; (N-CH_3, N-CH_2) creatine (- CH)Gly peak ratio; (- CH_3) Ala were useful assignments and NMR visible. The (N-CH_2, S-CH_2) taurine/(N-CH_3) PC: (- CH_3)Ala ratio were less NMR visible (see Figure 7). Unassigned peak near 3.1 ppm, were present in higher ratio (reference to Ala).

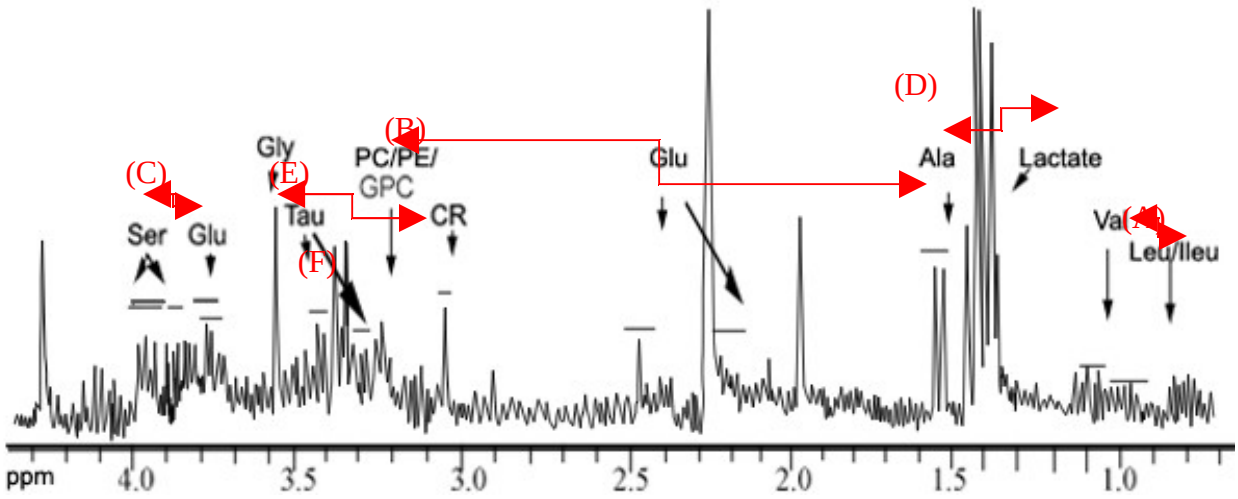

Figure 7: The H1-NMR assignments are shown with peak ratio of different phospholipids of skin in perchloric acid extract of normal skin tissue. The peaks showed up at 1 ppm region, (- , ' - CH_3)Val: (- , ' - CH_3)Leu/Ile peak intensity ratio = 1.2(A); (N-CH_3)PC/(N-CH_3)GPC:(- CH_3) Ala ratio = 0.60(B); (- CH) Glu: (- , - CH) Ser peak ratio = 1.3 (C); (- CH_3) lactate: (- CH_3) Ala ratio = 2.3 (D); (N-CH_3, N-CH_2) creatine (- CH):Gly peak ratio = 0.5 (E); (- CH_3) Ala were useful assignments and NMR visible. The (N-CH_2, S-CH_2) taurine/(N-CH_3) PC: (- CH_3)Ala ratio were less NMR visible (F).

Discussion

A preliminary study of human skin MRI characteristics with possibility of different skin age testing indicated the potential of microimaging as applicable to *in vivo* clinical MRI of skin. The *ex vivo* MRM identified and quantified skin components and area of hair body with viable epidermis. MRI data and histology data showed correlation between measurements of epidermis layer thickness, epidermis area, % "swollen epidermis burden" and hair follicle size. Present study adds new information of skin MR characteristics and possibility of contrast and resolution enhancement using optimization of MRI scan parameters and comparison of MRI-histopathological quantitation for human skin morphometric features. In addition, a simple method of skin age testing and skin typing showed the distinct textures, topography of skin surface.

The outermost layer of stratum corneum was brighter (= 450 micrometers thick) at SNR = 35. The next layer was epidermis at SNR = 15 appeared darker. Other next layer was collagen rich

dermis at SNR = 7 appeared dark. These layers showed the similar MRI signal intensities as in previous report [11]. The changes in MRI features of skin epidermis support the fragile nature of epidermis that is easily degenerated and swollen after loosing viability. This important MRI visible feature of skin epidermis has significant value in defining the quality of skin in degenerative skin diseases. Other important MRI visible feature of skin was hair follicle and its hair root with implications in assessment of skin growth.

Skin dermis is collagen rich made of two types: papillary and reticular dermis. The thin papillary dermis is more cellular, rich in fibroblasts and collagen-type III with less densely packed collagen. It showed high MR intensity similar with previous reports [1, 8]. Other different cell layers in dermis were made up of different cells and molecules of lipid, proteins, blood components, oil, sweat etc. These features amount to hypointensity due to reduced cell density and short T2 relaxation times of collagen-bound water in dermis at short echo time in corroboration with previously reports [4,8]. At short echo, SNR gain is about 100% and T2 = T2*. Other factor of susceptibility-induced gradients show artifacts at the air-tissue interface makes skin tissue components indistinguishable by MRI due to poor sensitivity and resolution. At high resolution, signal attenuation shows irreversible loss from diffusion through the imaging gradients as highlighted in previous report [2]. In our study, signal attenuation was not significant due to low T2 relaxation constants of epidermis and dermis (T2 = 20-35 msec). In previous study, T2* from dermis at echo times = 2.8-20 msec were shown to fit a monoexponential model (T2* $\pm$ sd= 12 $\pm$

1.4 msec) and the need of second minor component at echo time = 60 msec [3]. Other studies reported bi-exponential fit to T2* MR data (fast component = 9.8 msec for 91% total signal from collagen fiber type-II bound water; and slow component = 42.7 msec for less tightly bound water) [4,8,12]. The dense collage network in dermis also restricts diffusion.

In present study, at 500 MHz, stronger gradients allowed short phase encoding periods and read-out dephasing pulse widths to achieve short echo times using + 5 kHz bandwidth, 512-point receiver filter to acquire data in approximately 6 msec from readout to echo center. At high magnetic field, the use of high bandwidth receivers at short readout time may also reduce echo time and low-order phase correction to reconstruct the image using fractional echo [5]. However, high bandwidth induced noise can be offset by reduced T2* decay. Shorter readout time also reduced point spread function blurring at short T2*. Other benefit of high 500 MHz magnetic field was to achieve 20 micrometers in-plane resolution at readout gradient strength of 15 mT/meter for collecting 512 points at maximum band width $\pm$ 5 kHz to get high SNR (SNR is proportional to frequency$^{7/4}$) as described in previous study [12]. The present study indicated distinct delineation

of fat containing sebaceous gland and hypodermis structures. The increased SNR was significant considering that noise depends on square root of resistance and temperature. For argument, a nitrogen cooled radiofrequency coil (77 K) can enhance SNR by 3 times if coil is set at one place. In previous studies, the axial resolution of 11 micrometers and lateral resolution of 30 micrometers was reported for 2-3 mm skin depth [8,13]. However, MRI microimager offers high contrast of soft tissues perpendicular to skin surface with information of chemical makeup which causes modulation of relaxation times T1 and T2 [1]. The authors used one axis planar gradient insert to measure T1/T2 relaxation constants, proton density with hydration profile of skin layers in vivo within voxel size 18 x 312x 1000 micrometers [14]. The major drawback was large pixel size in second and third dimensions within large voxel size. Further, it remains challenge to get high detection sensitivity to offset the concomitant loss of signal-to-noise ratio (SNR). Main impediments are: low proton density and short T2 relaxation constant of dermis due to collagen bound water; and the skin heterogeneous nature; fast water relaxation in dermis; chemical shift misregistration at dermis-hypodermis interface in frequency direction at lower band width. Earlier, pixel shift of $\pm$ 14 KHz was reported at low band widths. Two options either fat suppression in sequence or using readout gradient polarity showed improved images keeping fat shifted away from dermis. Both these factors affect the MR visibility and may make routine skin magnetic resonance imaging inconclusive for determination of skin tissue composition, distinguishing fibrous rich and oil rich regions, viable and nonviable epidermis layers [11]. As a result, there has been considerable interest in the use of MRI and MRM for the noninvasive assessment of skin by

using gradient echo [5] and chemical shift microimaging [15]. Both sequences use fractional echo data collection from asymmetric FOV in read-out direction. The FLASH sequence was less sensitive to possible susceptibility induced field inhomogeneities near skin surface. The selection of flip angle = 150˚ was near the Ernst angle optimized for TR and T1 relxation constants (= 900 ms) of dermis similar to previous report [16]. Multislice multiecho MRM techniques can evaluate skin tissue composition and MRI characteristics of viable or nonviable epidermis better. 3D spin echo technique is promising technique to visualize continuously whole skin slab in all directions [5, 12-15]. The present study evaluates these observations. Due to paucity of sufficient information on *in vivo* MR skin image characterization, *ex vivo* MR image data validation was needed for skin.

The present study demonstrates the possibility of *in vivo* MR imaging accuracy in determination of epidermis and hair structure morphology in skin. It further highlighted the skin tissue characterization and components using 0.5 mm MR slice registration with 4-micron histology section. Epidermis, dermis, hair and sebaceous glands were measurable by using ex vivo MRI more

accurately than previous reports [12-15]. The MR visibility was based upon our earlier reported assumption that tissue components viz. lipid, collagen, fibrin, oil, sweat, vessels, cholesterol show different T1, proton density and T2 signal intensities depending upon their chemical structure and relaxation constants as shown in Table 7 [5, 17].

Multi-contrast approach identified dense stratum corneum as multilayer brighter glycolipid rich and viable epidermis as thin gray layer regions of human skin. Skin epidermis appeared as less dense as corroborating with earlier reports [5, 17]. Our data using 2D multi slice-multi echo short TE, long TR proton density weighted MRM confirm the sensitivity of MRI technique to skin proton density in the evaluation of skin hair quality and skin epidermis thickness (SET) as reported earlier [5, 17]. Our MRI results did not demonstrate skin vascularity and measurable degree of hair follicle on skin images. It confirms the previous reports [1,8,12] on distinct brighter stratum corneum, thin darker epidermis and hair follicle with grayish dense dermis with high protein and vascularized regions and oil-rich brighter sebaceous gland. However, the skin image MR signal properties of each skin component are poorly known [2,5,8,12].

At 11.7 T, in-plane resolution of 512 x 256 micrometers using 3D FLASH technique distinguished the skin components in 3D MRM skin slab e.g. lipid-rich protons, fibrous tissue appearing as brighter, hair follicle and hair root appearing as darker, and measured the size of epidermis thickness, hair follicle, and hair body area. However, 3D MSME technique showed better edges with more signal-noise ratio on images of skin appendages then 3D FLASH

technique. The histological specimen shrinkage caused underestimation of hair body area, hair follicle area and epidermis if compared with true measurements.

In coronal plane, magnetic resonance imaging showed contrast enhancement by using T1 and T2 different preparation phases and fat-suppressed gradient echo images. Proton density weighted and T2 weighted MRM images at different levels of brightness provided high SNR and distinct skin components. Most investigators reported spin-echo sequences for skin epidermis showing darker protein rich zone and lighter lipid rich stratum corneum tissue by T2 weighted sequences [1,2,5,11]. However, T2-weighted hypointensity and T1-weighted hyperintensity of vascular and fibrous dermis tissue possibly made distinction of vascular, fibrous tissue and oil rich glands [15-16]. In present report, lipid rich regions and fibrous content in dermis with epidermis and hair images generated optimized contrast at different TE and TR values. Present study corroborates with earlier observations of T2 weighted contrast using broad range of TR and TE values [5,17].

Parametric imaging for segmentation and quantification of MRI visible skin components based on their TE and TR values could be accomplished with high degree of sensitivity and specificity.

These TE/TR optimized values appeared to provide information using noninvasive ex vivo application of MRI criteria. T2-weighted signal intensities micro-dissected the hair body at different sets of TE values. However, T2-weighted images showed dermis region and fibrous components as darker. T1 weighted images provided less information than T2 weighted images or proton density weighted images. So, it needs appropriate TE and TR optimized choice for T2-weighted *in vivo* MR microimaging application.

Skin typing and grading were based mainly on two skin structures epidermis thickness and hair follicle size. These structures also change with age. Other skin chemicals such as collagen fiber, biochemical enzyme activities, macrophage function change and reflect skin age. The skin texture, topography, contour analyses of skin have been reported as tools of skin surface analysis with potentials in skin typing and grading the skin in dermatological evaluation and becoming noninvasive tools of skin age screening. Other several techniques have been reported but all these imaging methods remain still semi-quantitative. In present study, we attempted to identify differences of skin surface characteristics such as tonicity (skin mechano-sensory property), texture (softness), skin shape (lifted skin due to collagen or wrinkles) by texture, contour analysis. With age, differences in these visual skin properties are likely to serve the 'skin testing' or skin aging effects with possibility of monitoring the of effects of natural health products or drugs.

Amino acid resonance assignment peaks in the spectra of normal skin extracts were identified based on their chemical shifts, pH titration behaviors, molecular connectivity (coupled resonances)

and homonuclear splitting patterns, and relative peak intensities. The resonance peak ratios as molecular signatures of skin structures are not established yet as biomarkers.

What is innovative and novelty in present proposed study?

In vivo MR microimaging of skin on clinical MRI scanner has potential to distinguish the skin structures, their chemical nature and morphometric quantitation in different skin tissues from different age groups. MR microimaging may offer as noninvasive molecular imaging tool to monitor skin age, rapid monitoring of skin change by disease or drug therapy.

Limitations of the study:

The comparative analysis of skin structures in MRI images with those in histological sections showed measurable differences. The fresh frozen tissue histology technique suffers from shrinkage in skin size. This results in tissue shrinkage and shape deformation, which may lead to underestimation of the true lumen size. Furthermore, the ex vivo human skin is also subject to shrinkage lengthwise after dissection. The accuracy of skin hair length estimation by 4 micron

histology section was further compromised with the estimation of the hair length from the ends of the 0.5-mm skin MRI slices. It needs correction factor to minimize the impact of shrinkage. Other previous reports suggested that the lipid-rich content in hypodermis with viable epidermis were important factors in determining skin viability and early epidermal degeneration or melanoma [2,5,15]. However, differentiation of lipids from fibrous or heterogeneous dermis components of skin with the use of MRI is difficult because of the large pixel size compared with smaller size of skin structures. In the vicinity of skin dermis region, the magnetic resonance signal void was minimal on MSME spin-echo images due to no turbulence and resulted high signal-to-noise ratio with less contrast details. Availability of intradermal MRI micro-coils may enhance the chance of better skin characterization. Unfortunately, such technical advanced modifications are both invasive and expansive, therefore, less promising. Other possible improvements of MRI techniques such as diffusion weighting, high gradient strength, and a combination of T2-weighted imaging have been reported [12,18]. In *in vivo* MRI imaging, major limitations of getting high resolution are SNR, subject and physiological motion artifacts as these are determined by motion of skin (imaging volume) with respect to gradient isocenter. The technical developments and advances may help to determine skin viability and its type by MR microimaging.

Conclusion

In a human skin, the study demonstrated the multicontrast approach of ex vivo MRI microscopy (at 15 mTesla/meter in VOI 0.002 mm^3) at short echo time to determine the epidermis status as

skin viability, hair follicles with sebaceous gland as skin quality, hair body size and its accuracy by comparing measurements on histology sections.

Acknowledgements

Author acknowledges the instrument support for this pilot imaging data initially set up at FAMU-FSU College of Engineering, Tallahassee, FL with Dr Steven Gibbs and Dr Michael Peters and later approval of Dr Bruce R Locke. Author also acknowledges the courtesy for Figure 1 in this manuscript as part of skin MRI pilot study. Author acknowledges the coil characteristics and image computer analysis support of programmer Mr. Hitesh Trivedi by contract for access to his lab and computer analysis facility.

References

1.Bittoun J, Saint-Jalmes H, Querleux BG, Darrasse L, Jolivet O, Idy-Peretti I, Wartski M, Richard SB, Leveque JL. In vivo high-resolution MR imaging of the skin in a whole-body system at 1.5 T Radiology 1990; 176, 457-460.

2.Song HK, Wehrli FW. Variable TE gradient and spin echo sequences for in vivo MR microscopy of short T2 species. Magn Reson Med. 1998;39(2):251-8.

3.Kinsey ST, Moerland TS, McFadden L, Locke BR. Spatial resolution of transdermal water mobility using NMR microscopy. Magn Reson Imaging. 1997;15(8):939-47.

4.Knauss R. Fleischer G, Gründer W, Kärger J, Werner A. Pulsed field gradient NMR and nuclear magnetic relaxation studies of water mobility in hydrated collagen II. Mag Res Med 1996, 36, 241-248.

5.Sharma R. Microimaging of hairless rat skin by magnetic resonance at 900 MHz. Magn Reson Imaging. 2009;27(2):240-55.

6.Ma J, Wehrli W, Song HK Fast 3D large-angle spin-echo imaging(3D FLASH)Magn Reson Med 1996;35, 903-910.

1.Kim IH, Jo HY, Cho CG, Choi HC, Oh CH. Quantitative image analysis of hair follicles in alopecia areata. Acta Derm Venereol. 1999;79(3):214-6.

2.Denis A, Loustau O, Chiavassa-Gandois H, Vial J, Lalande Champetier de Ribes C, Railhac JJ, Sans N. High resolution MR imaging of the skin: normal imaging features. J Radiol. 2008;89(7-8 Pt 1):873-9.

3.Kim YH, Oreberg EK, Faull KF, Wade-Jardetzky NG, Jardetzky O. 1H NMR spectroscopy: An Approach to evaluation of diseased skin in vivo. J Invest Dermatol 1989; 92:210-216.

4.Brix G, Heiland S, Bellemann ME, Koch T, Lorenz WL. MR imaging of fat-containing tissues: Valuation of two quantitative imaging techniques in comparison with localized proton spectroscopy. Magn Reson Imaging.1993;11(7), 977-991.

7.Song HK, Wehrli FW, Ma J. In vivo MR microscopy of the human skin. Magn Reson Med. 1997;37(2):185-91.

8.Aubry S, Casile C, Humbert P, Jehl J, Vidal C, Kastler B. Feasibility study of 3-T MR imaging of the skin. Eur Radiol. 2009;19(7):1595-603.

9.Hubert Gufler[1], Folker E. Franke[2] and Wigbert S. Rau[1] High-Resolution MRI of Basal Cell Carcinomas of the Face Using a Microscopy Coil . *AJR* 2007; 188:W480-W484.

10.Querleux B, Magnetic resonance imaging and spectroscopy of skin and subcutis. J Cosmet Dermatol. 2004;3(3):156-61.

11.Weis J, Astrom G, Vinnars B, Wanders A, Ahlstrom H. Chemical shift microimaging of subcutaneous lesions. MAGMA 2005;18:59-62.

12.Richard SB J Invest Dermatol. 1991; 97, 120-125

13.McDonald PJ, Akhmerov A, Backhouse LJ, Pitts S. Magnetic resonance profiling of human skin in vivo using GARField magnets.J Pharm Sci. 2005;94(8):1850-60.

14.Tran HV, Charleux F, Rachik M, Ehrlacher A, Ho Ba Tho MC. In vivo characterization of the mechanical properties of human skin derived from MRI and indentation techniques. Comput Methods Biomech Biomed Engin. 2007;10(6):401-7.

Rakesh Sharma